Liquid–Solid Mass Transfer for Cocurrent Gas–Liquid Upflow Through Solid Foam Packings

P. W. A. M. Wenmakers, J. van der Schaaf, B. F. M. Kuster, and J. C. Schouten
Laboratory of Chemical Reactor Engineering, Eindhoven University of Technology, 5600 MB Eindhoven, The Netherlands

DOI 10.1002/aic.12204
Published online June 22, 2010 in Wiley Online Library (wileyonlinelibrary.com).

This article presents the liquid–solid mass transfer characteristics for cocurrent upflow operated gas–liquid solid foam packings. Aluminum foam was used with 10, 20, and 40 pores per linear inch (PPI), coated with 5 wt % Pd on γ-alumina. The effects of gas velocity ($u_g = 0.1-0.8\ m_g^3\ m_r^{-2}\ s^{-1}$) and liquid velocity ($u_l = 0.02$ and $0.04\ m_l^3\ m_r^{-2}\ s^{-1}$) are studied using the Pd/Bi catalyzed oxidation of glucose. The volumetric liquid–solid mass transfer coefficient, $k_{ls}a_{ls}$, is approximately the same for 10 PPI and 20 PPI solid foams, ranging from 2×10^{-2} to $9 \times 10^{-2}\ m_l^3\ m_r^{-3}\ s^{-1}$. For 40 PPI solid foam, somewhat lower values for $k_{ls}a_{ls}$ were found, ranging from 6×10^{-3} to $4 \times 10^{-2}\ m_l^3\ m_r^{-3}\ s^{-1}$. The intrinsic liquid–solid mass transfer coefficient, k_{ls}, increases with increasing liquid velocity and was found to be proportional to $u_l^{0.98}$. Initially, k_{ls} decreases with increasing gas velocity and after reaching a minimum value increases with increasing gas velocity. The values for k_{ls} range from 5.5×10^{-6} to $8 \times 10^{-4}\ m_l^3\ m_i^{-2}\ s^{-1}$, which is in the same range as found for random packings and corrugated sheet packings. © 2010 American Institute of Chemical Engineers *AIChE J,* 56: 2923–2933, 2010

Keywords: chemical reactors, mass transfer, multiphase reactors, packed beds, solid foam

Introduction

For the design of chemical reactors, one has to deal with hydrodynamics, heat and mass transfer, and catalyst activity. For heterogeneously catalyzed reactions, the rate of the reaction is often limited by mass transfer instead of the intrinsic kinetics. The rate-limiting step can be the gas–liquid mass transfer, liquid–solid mass transfer, and intraparticle diffusion. These limitations reduce the overall conversion and selectivity of the process. The effect of mass transfer and diffusion limitation can be reduced by the application of a suitable packing as a catalyst support. Classically, so-called random packings have been used, e.g., porous spherical particles or Berl saddles. However, with structured packings, an even higher selectivity and conversion can be obtained. Different types of packings have been discussed in literature, i.e., monoliths,[1] Sulzer Katapak elements,[2,3] cloths,[4] and fibers.[5] A general review describing the different aspects of structured packings (e.g., pressure drop, mass transfer characteristics, residence time distribution) is given by Pangarkar et al.[6] The use of a (structured) packing also overcomes the cumbersome step of catalyst separation, which is often encountered in slurry reactors.

Another type of structured packing is the solid foam packing, a highly porous open celled material. The structure of the solid foam resembles the inverse of a packed bed of spherical particles.[7] The average cell size is often expressed in pores per linear inch (PPI). Solid foam is commercially available in a range of 5–100 PPI in a wide variety of materials, e.g., ceramics, metals, plastics, and carbon. The porosity of the solid foam ranges from 80 to 97%.

Stemmet et al.,[8–10] Twigg and Richardson,[11] and Garrido et al.[12] have shown that the pressure drop of solid foam is low compared to the pressure drop of conventional packed beds. Also, high gas–liquid mass transfer rates have been reported, $k_{gl}a_{gl}$ up to 0.6 $m_l^3\ m_r^{-3}\ s^{-1}$.[10] These high mass transfer rates have been attributed to the high interfacial area of the solid foam. In addition to the gas–liquid mass transfer rate, also the liquid–solid mass transfer is important in the design of gas–liquid–solid reactors. Only a limited amount

Correspondence concerning this article should be addressed to J. C. Schouten at j.c.schouten@tue.nl.

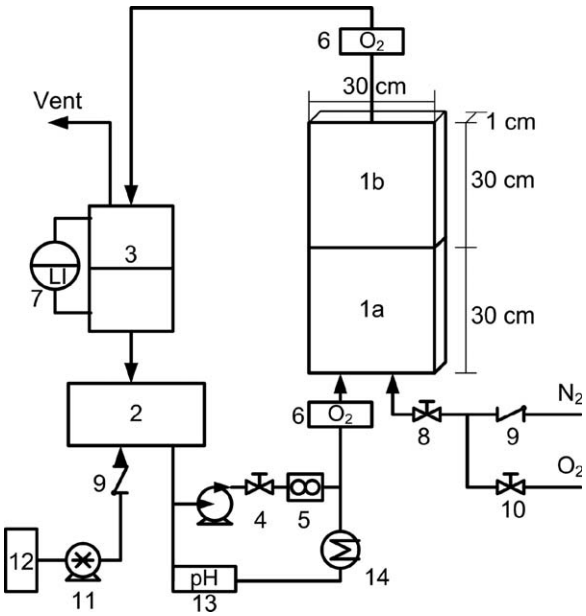

Figure 1. Schematical representation of the experimental setup.

(1) Two-dimensional solid foam packed bed; (2) main liquid supply vessel; (3) gas–liquid separator; (4) liquid flow control valve; (5) liquid mass flow controller; (6) dissolved oxygen sensor; (7) liquid level indicator; (8) gas mass flow controllers for each of the five distributor blocks; (9) check valve; (10) valve to switch from nitrogen to air; (11) sodium hydroxide dosing pump; (12) sodium hydroxide storage vessel; (13) pH controller; and (14) heat exchanger.

of literature is available for the liquid–solid mass transfer in gas–liquid operated structured packings. Higler et al.,[3] and van Baten and Krishna[13] have determined the liquid–solid mass transfer for KATAPAK-S® packings using computational fluid dynamics simulations. They found liquid–solid mass transfer coefficients ranging from 0.47×10^{-6} to 5.16×10^{-6} m_l^3 m_i^{-2} s^{-1}. Battista and Boehm[14] have measured the liquid–solid mass transfer for corrugated sheets using an electrochemical technique, values of k_{ls} ranging from 2.4×10^{-6} to 1.7×10^{-5} m_l^3 m_i^{-2} s^{-1} were reported[15] and have studied the liquid–solid mass transfer in liquid operated solid foam packings using an electrochemical technique. They found values of $k_{ls}a_{ls}$ ranging from 0.03 to 0.13 m_l^3 m_r^{-3} s^{-1} for solid foam of 45–100 PPI.

This work focuses on quantifying the liquid–solid mass transfer coefficient for cocurrent gas–liquid upflow through solid foam packings. The liquid–solid mass transfer coefficient is determined by using the Pd/Bi catalyzed oxidation of glucose. Solid foams washcoated with Pd/γ-alumina were used for the catalytic experiments. Solid foam pieces with different cell size were used (10 PPI, 20 PPI, and 40 PPI). The effect of liquid velocity, gas velocity, and cell size on the liquid–solid mass transfer coefficient has been studied.

Approach

Experimental setup

The volumetric liquid–solid mass transfer coefficient, $k_{ls}a_{ls}$, for cocurrent gas–liquid upflow through solid foams was determined using the setup shown in Figure 1. The setup consists of a pseudo two-dimensional column of 1×30 cm^2 cross sectional area, which can vary in height, either 30 cm or 60 cm high. Stemmet et al.[10] have shown that the gas–liquid mass transfer coefficient, $k_{gl}a_{gl}$, for solid foam packings can be determined by the desorption of a dissolved gas and measuring the dissolved gas concentration at the inlet and the outlet of the column. However, the obtained $k_{gl}a_{gl}$ contained contributions of the inlet and the exit. Stemmet et al.,[10] and Luo and Ghiaasiaan[16] show that by evaluating $k_{gl}a_{gl}$ for different packing heights, the contributions of the entrance and exit can be taken into account (see section "Entrance and exit effects").

The liquid–solid mass transfer coefficient for cocurrent gas–liquid upflow through solid foams was determined using the Pd/Bi catalyzed oxidation of glucose. For this, Pd/γ-alumina washcoated solid foam packings have been used. It is assumed that the contribution of the entrance is significantly larger than the contribution of the exit. The entrance contribution is the result of the injection of the gas into the liquid, the higher rate of turbulence, and the smaller size of the gas bubbles increases $k_{gl}a_{gl}$ and $k_{ls}a_{ls}$. The exit effect is caused by the additional mass transfer taking place between the column outlet and the position of the oxygen sensor. To eliminate the contribution of the entrance on the determination of $k_{ls}a_{ls}$, two 30-cm high solid foam pieces have been used. Only the solid foam piece on top (solid foam element 1b in Figure 1) was washcoated with Pd/γ-alumina. The solid foam piece at the bottom (solid foam element 1a in Figure 1) does not contain any catalyst, here only absorption of the oxygen into the liquid phase takes place.

A schematical representation of the different transport phenomena taking place at both the catalytic and noncatalytic solid foam piece is shown in Figure 2. The figure shows that for the quantification of $k_{ls}a_{ls}$, the gas–liquid mass transfer coefficient of the noncatalytic solid foam piece at the bottom of the column, $(k_{gl}a_{gl})_{L_1}$, and the gas–liquid mass transfer coefficient of the catalytic solid foam piece at

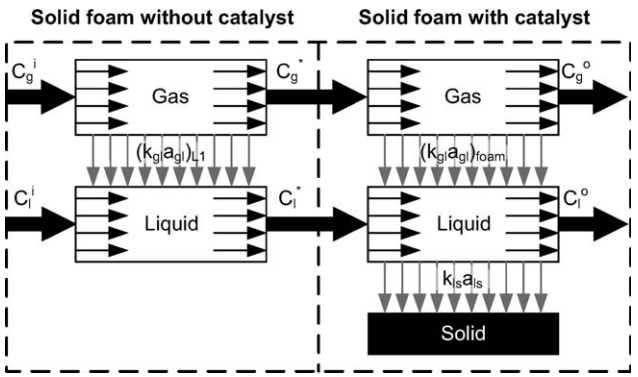

Figure 2. Schematical representation of the gas–liquid and liquid–solid mass transfer steps taking place during the determination of the liquid–solid mass transfer coefficient of the solid foam.

In the solid foam piece without catalyst, absorption of the gas takes place. In the solid foam piece with catalyst, competitive absorption and liquid–solid mass transfer to the catalyst take place.

the top of the column, $(k_{gl}a_{gl})_{foam}$, are required. The approach followed to determine the individual mass transfer coefficients $(k_{gl}a_{gl})_{L_1}$, $(k_{gl}a_{gl})_{foam}$, and $k_{ls}a_{ls}$ is described in the following sections.

Gas–liquid mass transfer

The mole balance describing the mass transfer in the column depends on the flow type of the individual phase, i.e., plug flow, ideally mixed, or axial dispersion. The gas phase moves at a high velocity through the column and is either present as bubbles or slugs. In both cases, the gas moves homogeneously through the column, thus the gas phase is assumed to be in plug flow. Stemmet et al.[10] determined the liquid phase axial dispersion using tracer experiments. The Bodenstein number exceeds 10 for all their experiments. The solid foam used and the range of gas and liquid velocities used by Stemmet et al.[10] encompasses the conditions used in this study. Stemmet et al.[10] have shown that assuming plug flow for the liquid phase introduces a small error in the determination of the value of the gas–liquid mass transfer coefficient. For a Bodenstein number of 10, the assumption of plug flow results in an underestimation of the gas–liquid mass transfer coefficient of at maximum 16%. Assuming plug flow for both the gas phase and the liquid phase, the (pseudo) steady state mole balances in case of gas–liquid mass transfer (viz. desorption/absorption) are:

$$-u_g \frac{dC_g}{dz} - k_{gl}a_{gl}\left(\frac{C_g}{H} - C_l\right) = 0 \quad \text{Gas phase} \tag{1}$$

$$-u_l \frac{dC_l}{dz} + k_{gl}a_{gl}\left(\frac{C_g}{H} - C_l\right) = 0 \quad \text{Liquid phase} \tag{2}$$

where u_g is the superficial gas velocity, C_g is the gas phase concentration, z is the spatial reactor coordinate, $k_{gl}a_{gl}$ is the volumetric gas–liquid mass transfer coefficient, H is the Henry coefficient, C_l is the liquid phase dissolved gas concentration, and u_l is the superficial liquid velocity. Using C_l^i and C_g^i as the initial conditions for the liquid phase and gas phase, respectively, the mole balances solve to[10]:

$$\ln\left(\frac{\frac{C_g}{H} - C_l}{\frac{C_g^i}{H} - C_l^i}\right) = -k_{gl}a_{gl}\left(\frac{1}{u_g H} + \frac{1}{u_l}\right)L \tag{3}$$

where L is the packing height. The volumetric mass transfer coefficient can thus be obtained from pseudo steady state dissolved oxygen concentrations. The value for the outlet gas concentration, C_g, can be obtained from the overall mole balance:

$$C_g = C_g^i + \frac{u_l}{u_g}\left(C_l^i - C_l\right) \tag{4}$$

Entrance and exit effects

The overall gas–liquid mass transfer coefficient determined from the experimental gas and liquid phase concentrations, using Eq. 3, is the average mass transfer coefficient for the complete height of the column. However, the injection of the gas into the liquid, at the bottom of column, results in a high degree of turbulence and the presence of small gas bubbles. The flow regime stabilizes along the length of the column. Also, the dissolved oxygen sensor at the exit of the column is located after the exit of the column (Figure 1), therefore, also mass transfer occurs after the column outlet. These entrance and exit effects increase the value of $k_{gl}a_{gl}$. Assuming that the entrance and exit effects are constant for given gas and liquid velocities, Stemmet et al.[10] and Luo and Ghiaasiaan[16] have shown that the entrance effect can be accounted for by evaluating the volumetric mass transfer coefficient for different packing heights. The gas–liquid mass transfer coefficient of the packing can be determined according to:

$$\left(k_{gl}a_{gl}\right)_{foam} = \frac{(k_{gl}a_{gl})_{L_1}L_1 - (k_{gl}a_{gl})_{L_2}L_2}{L_1 - L_2} \tag{5}$$

where $(k_{gl}a_{gl})_{foam}$ is the volumetric mass transfer coefficient without entrance and exit effects, and $(k_{gl}a_{gl})_{L_i}$ is the volumetric mass transfer coefficient for packing height L_i.

Liquid–solid mass transfer

In case of a catalytically active packing, the liquid–solid mass transfer and the reaction rate have also to be taken into account in the mole balances. The liquid phase mole balance for a catalytically active packing under steady state conditions is:

$$-u_l \frac{dC_l}{dz} + \left(k_{gl}a_{gl}\right)_{foam}\left(\frac{C_g}{H} - C_l\right) - k_{ls}a_{ls}(C_l - C_s) = 0 \tag{6}$$

where $k_{ls}a_{ls}$ is the volumetric liquid–solid mass transfer coefficient and C_s is the concentration at the liquid–solid interface. As a result of the low solubility of gases in liquids, typically 1 mol m_l^{-3} for pure oxygen in water under ambient conditions, only the transfer rate of the gaseous component needs to be considered. The liquid–solid interfacial concentration, C_s, can be determined from the expression for the reaction rate. In case of a (pseudo) first-order reaction, the reaction rate of the glucose oxidation is given by Kluytmans et al.[17] and Ruthiya et al.[18,19]:

$$R_v = \eta k_r L_t \rho_{sup} \varepsilon_{sup} C_s \tag{7}$$

where R_v is the reaction rate per unit of reactor volume, η is the effectiveness factor, k_r is the intrinsic reaction rate coefficient, L_t is weight specific amount of surface atoms of catalyst per weight of washcoat support, ρ_{sup} is the density of the support, and ε_{sup} is the holdup of the support. In steady state operation, the liquid–solid mass transfer rate, $k_{ls}a_{ls}(C_l - C_s)$, is equal to the chemical reaction rate, and the liquid–solid interfacial concentration, C_s, is determined as follows:

$$C_s = \frac{k_{ls}a_{ls}}{k_{ls}a_{ls} + \eta k_r L_t \rho_{sup} \varepsilon_{sup}} C_l \tag{8}$$

Combining Eqs. 1, 6, and 8 results in (see appendix A):

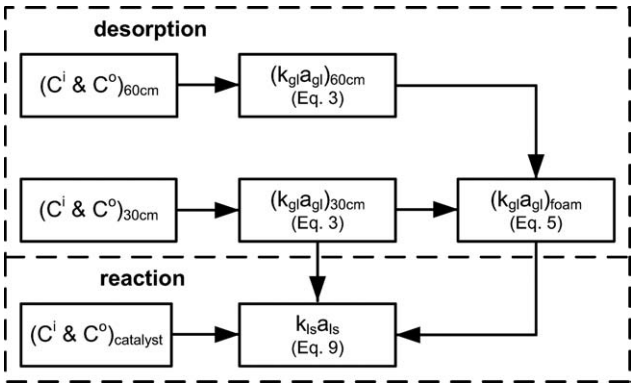

Figure 3. Schematical representation of the calculation scheme for the determination of the liquid–solid mass transfer coefficient.

$$C_l = e^{-\frac{1}{2}(\alpha+\beta)z}\left[C_l^m \cos h\left(z\sqrt{\frac{1}{4}(\alpha+\beta)^2+\alpha(\gamma-\beta)}\right)+\ldots \left(\frac{1}{2}C_l^m(\alpha-\beta)+\frac{C_g^m}{H}\gamma\right)\frac{\sin h\left(z\sqrt{\frac{1}{4}(\alpha+\beta)^2+\alpha(\gamma-\beta)}\right)}{\sqrt{\frac{1}{4}(\alpha+\beta)^2+\alpha(\gamma-\beta)}}\right] \quad (9)$$

with:

$$\alpha = \frac{k_{gl}a_{gl}}{u_g H} \quad (10)$$

$$\beta = \frac{k_{gl}a_{gl}}{u_l} + \frac{k_{ls}a_{ls}}{u_l}\left(1 - \frac{k_{ls}a_{ls}}{k_r L_t \rho_{sup}\varepsilon_{sup} + k_{ls}a_{ls}}\right) \quad (11)$$

$$\gamma = \frac{k_{gl}a_{gl}}{u_l} \quad (12)$$

where C_l^m is the liquid phase dissolved gas concentration and C_g^m is the gas phase concentration, both at the inlet of the catalytic solid foam piece, see Figure 2.

The liquid–solid mass transfer coefficient can be calculated using the steady-state concentrations obtained from experiments with catalytically active solid foam pieces, see Figure 3. The values of C_l^m and C_g^m are calculated using Eqs. 3 and 4, using the gas–liquid mass transfer coefficient obtained for one piece of solid foam, $(k_{gl}a_{gl})_{L_t}$. This includes the entrance effects into the values of C_l^m and C_g^m. For the catalytic solid foam section, the gas–liquid mass transfer coefficient of the solid foam, $(k_{gl}a_{gl})_{foam}$, is used.

Experimental

Materials

The solid foams used in this study are commercially available under the brand name Duocell (ERG Materials and Aerospace). Figure 4 shows images of aluminum foam of 10, 20, and 40 PPI. All the foams used in this study have a voidage of 92–94% and are 30 × 30 × 1 cm^3 in size. Aluminum foam pieces of 10, 20, and 40 PPI have been coated by Johnson Matthey with 18.7 ± 0.3 g of 5 wt % Pd on γ-alumina. The dispersion of the catalyst was supplied by Johnson Matthey and is 30–35%. The palladium was reduced to its metallic state using an aqueous 5 mole sodium borohydride (Sigma-Aldrich, ≥98.5%) per mole Pd solution. The Pd/γ-alumina washcoated foam was submerged in the vigorously stirred aqueous sodium borohydride solution for 1 h. The palladium catalyst was promoted with Bi with a ratio of 5 mol Pd/mol Bi as described by Ruthiya.[19] Sodium hydroxide (Merck, >97%) and D-glucose (Merck, biochemistry grade) were used for kinetic tests.

Setup

The foam pieces were placed in a pseudo two-dimensional column with varying height, either 30 or 60 cm high, and a cross section of 30 × 1 cm^2, see Figure 1. Air or nitrogen is used as the gas phase and a 0.5 mol L glucose solution in demineralized water is used as the liquid phase. The gas and the liquid are flowing cocurrently upward. The liquid enters the bottom of the column through five distributor holes placed evenly along the width of the column. The flow is measured and controlled using a coriolis flow meter (Rheonik) and a control valve (Badger Meter). The gas enters the column through five distributor blocks each with 20 holes of 0.5 mm in diameter. The gas flow towards each of the distributor blocks is controlled by five individual thermal mass flow controllers (Brooks). The ranges of gas and liquid velocities used in this study are 0.1–0.8 $m_g^3\ m_r^{-2}\ s^{-1}$ and 0.02–0.04 $m_l^3\ m_r^{-2}\ s^{-1}$, respectively. The liquid is recycled via a gas–liquid separator back to the supply vessel. In the gas–liquid separator, the liquid level is measured to determine the liquid holdup in the column containing the solid foam. The liquid temperature is

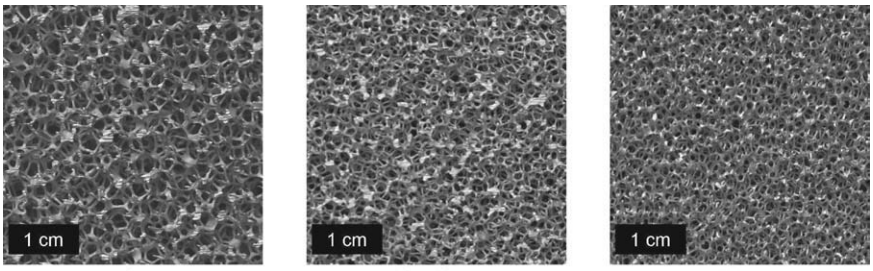

(a) 10 PPI (b) 20 PPI (c) 40 PPI

Figure 4. Detail of 10, 20, and 40 PPI aluminum foams (ERG Material and Aerospace, Duocel) showing the reticulated network of struts with its high voidage.

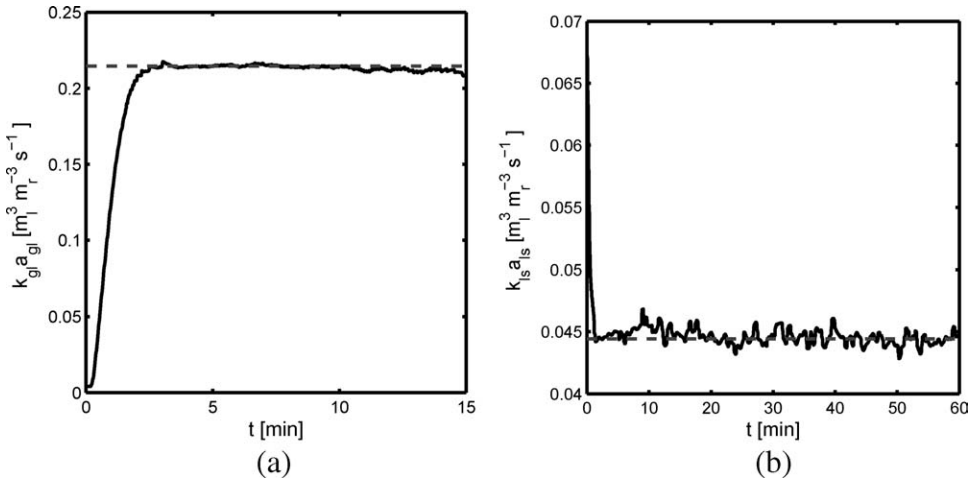

Figure 5. Calculated gas–liquid and liquid–solid mass transfer coefficients as a function of time for 60 cm 10 PPI foam with $u_g = 0.02$ m_g^3 m_r^{-2} s^{-1} and $u_l = 0.04$ m_l^3 m_r^{-2} s^{-1}.

(a) The solid line shows $k_{gl}a_{gl}$ as a function of time. Initially, $k_{gl}a_{gl}$ increases monotonously. After ~2 min, $k_{gl}a_{gl}$ is constant and the system has reached pseudo steady state. The dashed line indicates the average value during the period that $k_{gl}a_{gl}$ is constant. (b) The solid line shows the calculated $k_{ls}a_{ls}$ as a function of time. Initially, there is a sharp change in the value of $k_{ls}a_{ls}$ after which it slowly decreases to its steady state value. After ~20 min, the value of $k_{ls}a_{ls}$ is stable and the system has reached steady state. The dashed line indicates the average value of $k_{ls}a_{ls}$ during the steady state.

maintained at 48.7°C ± 0.5°C. The pH of the system is maintained at 9 during the reaction using a pH electrode (Hanna Instruments, HI 61014), a pH controller (Hanna Instruments, PH500), and a dosing pump adding a 5 mol/L sodium hydroxide aqueous solution to the system.

Holdup

The liquid holdup was determined by completely filling the column with liquid and measuring the liquid level in the gas–liquid separator. Next, the gas is fed to the column and the flow is allowed to stabilize for 3 mins. The amount of liquid expelled by the gas phase is determined by measuring the liquid level in the gas–liquid separator. The liquid-holdup is determined by subtraction of the amount of expelled liquid for 30 cm and 60 cm of solid foam.

Gas–liquid mass transfer

The gas–liquid mass transfer coefficient was determined by means of oxygen desorption with nitrogen. For the determination of the gas–liquid mass transfer coefficient, solid foam pieces without catalyst have been used. First, the liquid is saturated with oxygen after which the inlet gas is switched from air to nitrogen. The dissolved oxygen concentration of the inlet and outlet was measured using InPro6800 oxygen sensors (Mettler Toledo). The inlet concentration of the liquid phase will gradually drop during the experiment as a result of the recycling of the liquid phase.

The gas-mass liquid mass transfer coefficient was calculated from the measured dissolved oxygen concentrations at the inlet and outlet using Eqs. 3 and 4. Figure 5a shows $k_{gl}a_{gl}$ as a function of time. The solid line represents $k_{gl}a_{gl}$ and the dotted line represents the average value of $k_{gl}a_{gl}$ during pseudo steady state. Initially, $k_{gl}a_{gl}$ increases with time, after a few minutes it levels off to a constant value. The constant value of $k_{gl}a_{gl}$ shows that the pseudo steady state assumption of Eq. 3 is valid. After ~10 mins, $k_{gl}a_{gl}$ starts to decrease. This is the result of the low dissolved oxygen concentration at the exit of the reactor. The dissolved oxygen concentration is now within the error of the sensor, which yields erroneous results.

Liquid–solid mass transfer

The liquid–solid mass transfer coefficient was determined by means of the Pd/Bi catalyzed oxidation of glucose. The influence of entrance effects on the determination of the liquid–solid mass transfer coefficient was taken into account by equipping the column with two pieces of solid foam. A piece of foam without catalyst was inserted at the bottom of the column and a piece of foam with catalyst was inserted at the top of the column (see Figure 1). First, a gas flow of nitrogen was set after which the liquid was heated to the reaction temperature. After reaching the reaction temperature, the gas phase was switched from nitrogen to oxygen. These settings are maintained for 1 h in which the reaction is allowed to take place to reach steady state conditions.

The liquid–solid mass transfer coefficient was calculated using Eq. 9 according to the scheme shown in Figure 3. Figure 5b shows $k_{ls}a_{ls}$ as a function of time. Initially, there is a rapid change in $k_{ls}a_{ls}$ after which it slowly stabilizes, except for some noise. The constant value of $k_{ls}a_{ls}$ shows that the pseudo steady state assumption of Eq. 9 is valid.

Results and Discussion

Gas–liquid mass transfer

The gas–liquid mass transfer coefficient of the solid foam, $(k_{gl}a_{gl})_{foam}$, was determined by using Eq. 5. Figure 6a shows $(k_{gl}a_{gl})_{foam}$ as a function of the gas velocity. The open symbols correspond to $u_l = 0.02$ m_l^3 m_r^{-2} s^{-1} and the closed symbols correspond to $u_l = 0.04$ m_l^3 m_r^{-2} s^{-1}. The dashed

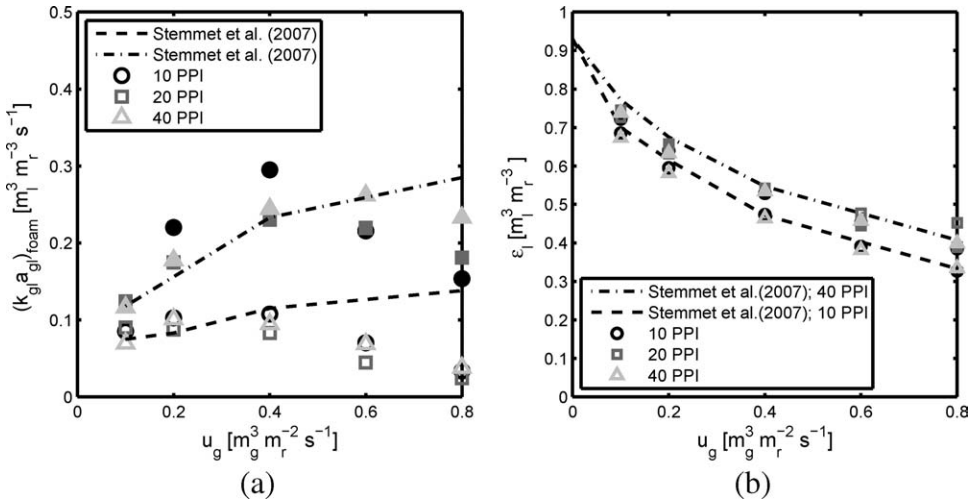

Figure 6. Gas–liquid mass transfer coefficient and liquid holdup as a function of gas velocity.

The open symbols correspond to $u_l = 0.02$ m_l^3 m_r^{-2} s^{-1} and the closed symbols correspond to $u_l = 0.04$ m_l^3 m_r^{-2} s^{-1}. The dashed line corresponds to the data of Stemmet et al.[10] for $u_l = 0.02$ m_l^3 m_r^{-2} s^{-1} and the dash–dot line corresponds to the data of Stemmet et al.[10] for $u_l = 0.04$ m_l^3 m_r^{-2} s^{-1} for 40 PPI. (a) The gas–liquid mass transfer coefficient increases with increasing liquid velocity. $k_{gl}a_{gl}$ shows a maximum as a function of gas velocity. For lower gas velocities, $k_{gl}a_{gl}$ corresponds well with the data of Stemmet et al.[10] (b) The liquid holdup decreases with increasing gas velocity and is in the same range as measured by Stemmet et al.[10]

line and the dash–dot line correspond to the data obtained by Stemmet et al.[10] for 40 PPI solid foam for a liquid velocity of 0.02 m_l^3 m_r^{-2} s^{-1} and 0.04 m_l^3 m_r^{-2} s^{-1}, respectively, using an air–water system. For low gas velocities, $(k_{gl}a_{gl})_{foam}$ corresponds within 22% to the data obtained by Stemmet et al.,[10] except for 10 PPI at a liquid velocity of 0.04 m_l^3 m_r^{-2} s^{-1}. The strut thickness of the solid foam is the highest for 10 PPI solid foam. Therefore, the degree of turbulence at the entrance is the highest for the 10 PPI solid foam. This turbulence, or entrance effect, results in higher mass transfer rates. This introduces some error in the quantification of $k_{gl}a_{gl}$.

For gas velocities higher than ~0.4 m_g^3 m_r^{-2} s^{-1}, the values of $(k_{gl}a_{gl})_{foam}$ start to decrease. A similar effect was observed by Stemmet et al.[10] for 10 PPI solid foam at a liquid velocity of 0.02 m_l^3 m_r^{-2} s^{-1}. They attributed this to the local depletion of the liquid film which is present on the solid foam inside a gas bubble. In this work, the temperature of the liquid is 50° instead of 30° as in the work of Stemmet et al.,[10] resulting in a lower gas solubility. Therefore, the measurement of the gas–liquid mass transfer coefficient is more prone to local depletion, resulting in lower values of the gas–liquid mass transfer coefficient. The use of these lower gas–liquid mass transfer coefficients for the determination of $k_{ls}a_{ls}$ would lead to an underestimation of $k_{ls}a_{ls}$. Therefore, the gas–liquid mass transfer coefficients of Stemmet et al.[10] have been used to obtain $k_{ls}a_{ls}$ for those cases where $(k_{gl}a_{gl})_{foam}$ decreases with increasing gas velocity.

Figure 6 shows the liquid holdup as a function of gas velocity. The open symbols correspond to $u_l = 0.02$ m_l^3 m_r^{-2} s^{-1} and the closed symbols correspond to $u_l = 0.04$ m_l^3 m_r^{-2} s^{-1}. The dash–dot lines correspond to the maximum and minimum values of ε_l as obtained by Stemmet et al.[10] for 10 and 40 PPI solid foam using an air–water system. The graph shows that ε_l decreases with increasing gas velocity. For $u_l = 0.04$ m_l^3 m_r^{-2} s^{-1}, the liquid holdup is approximately the same for all PPI numbers. The deviation from the average value is less than 2%. For $u_l = 0.02$ m_l^3 m_r^{-2} s^{-1}, the liquid holdup is the same for 10 and 40 PPI solid foam, with a deviation from the average value which is less than 1.2%. For 20 PPI solid foam, a higher liquid holdup is found and deviates up to 30% from the average value of 10 and 40 PPI solid foam. The ε_l found in this work is in the same range as found by Stemmet et al.[10] For cocurrent upflow gas–liquid packed bed reactors, the liquid holdup typically increases with increasing liquid velocity and decreasing gas velocity.[20] Stemmet et al.[10] found that the liquid holdup for solid foams changes slightly with varying liquid velocity. However, no significant trend is observed between the liquid velocity and the liquid holdup.

Liquid–solid mass transfer

Figure 7a shows $k_{ls}a_{ls}$ as a function of liquid velocity. The open symbols with solid lines correspond to $u_l = 0.02$ m_l^3 m_r^{-2} s^{-1} and the closed symbols with dashed lines correspond to $u_l = 0.04$ m_l^3 m_r^{-2} s^{-1}. The graph shows that $k_{ls}a_{ls}$ is significantly lower for 40 PPI than for 10 and 20 PPI, which are approximately the same. On average, $k_{ls}a_{ls}$ for 40 PPI is 54% lower than for 10 and 20 PPI. The specific surface area of the solid foam is proportional to the PPI number (see Eq. 14). This means that the intrinsic liquid–solid mass transfer coefficient, k_{ls}, decreases with increasing PPI number. Approximately, the same behavior was observed by Wenmakers et al.[21] for the single phase liquid–solid mass transfer using carbon nanofiber (CNF) covered solid foam packings. They observed significantly higher liquid–solid mass transfer rates for 20 PPI CNF covered solid foam than for 45 and 60 PPI CNF covered solid foam. This is because the 20 PPI foam generates more turbulence; the strut thickness of the solid foam increases with decreasing PPI number and thicker struts generate more turbulence. Figure 7a shows that $k_{ls}a_{ls}$ increases with increasing liquid velocity, this shows that the higher refreshment rate of the struts by the liquid phase increases $k_{ls}a_{ls}$.

Figure 7a shows that $k_{ls}a_{ls}$ initially decreases with increasing gas velocity, but after reaching a minimum value $k_{ls}a_{ls}$

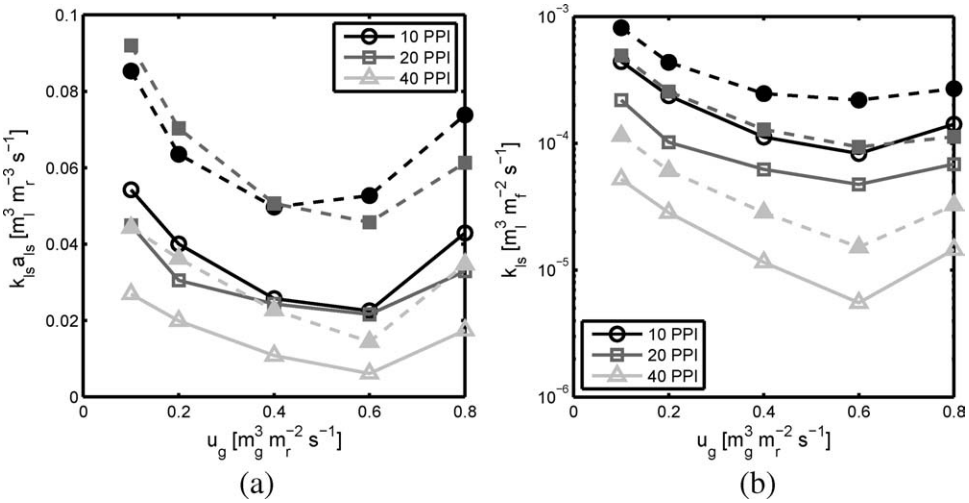

Figure 7. Liquid solid mass transfer coefficient as a function of the gas velocity.

The open symbols with the solid lines correspond to $u_l = 0.02$ m_l^3 m_r^{-2} s^{-1} and the closed symbols with the dashed lines correspond to $u_l = 0.04$ m_l^3 m_r^{-2} s^{-1}. (a) The liquid–solid mass transfer coefficient is approximately the same for 10 and 20 PPI solid foam. For 40 PPI, a lower $k_{ls}a_{ls}$ is observed. $k_{ls}a_{ls}$ increases with increasing liquid velocity. For all cases, a local minimum is observed as a function of gas velocity. (b) The intrinsic liquid–solid mass transfer coefficient, k_{ls}, initially decreases rapidly with increasing gas velocity. k_{ls} also shows a local minimum.

increases with increasing gas velocity. If the liquid–solid mass transfer takes place through the thin liquid film which is present on the solid-foam inside the gas bubbles, this effect of gas velocity can be related to the increase in the gas holdup. Assuming that liquid–solid mass transfer mainly takes place within the gas bubbles, the intrinsic mass transfer coefficient, k_{ls}, can be determined as follows:

$$k_{ls} = \frac{k_{ls}a_{ls}}{a_f \varepsilon_g} \tag{13}$$

where a_f is the specific surface area of the solid foam and ε_g is the gas holdup. The specific surface area is determined by using the geometric tetrakaidecahedron model as described by Incera Garrido et al.,[12] where D_p is approximated by $25.4 \times 10^{-3}/N_{PPI}$:

$$a_f = \frac{4.82}{D_p}\sqrt{1-\varepsilon_f} \approx 190 N_{PPI}\sqrt{1-\varepsilon_f} \tag{14}$$

Figure 7b shows k_{ls} as a function of gas velocity. The graph shows that k_{ls} decreases rapidly with increasing gas velocity. k_{ls} shows a minimum as was observed for $k_{ls}a_{ls}$. Apparently, $k_{ls}a_{ls}$ is not solely determined by the gas holdup. Probably different liquid–solid mass transfer steps are present in this system, e.g., liquid–solid mass transfer taking place through the thin liquid film present on the solid foam inside the gas bubble and liquid–solid mass transfer taking place within the bulk liquid outside the gas bubbles. The liquid–solid interfacial area, a_{ls}, is the area available per unit of reactor volume, the liquid–solid interfacial area per unit of gas or liquid volume can be obtained as follows:

$$a_{ls}^g = \frac{a_{ls}}{\varepsilon_g} \quad \text{or} \quad a_{ls}^l = \frac{a_{ls}}{\varepsilon_l} \tag{15}$$

where a_{ls}^g and a_{ls}^l are the specific liquid–solid interfacial area per unit gas volume and unit liquid volume, respectively. The measured $k_{ls}a_{ls}$ consists of a combination of the liquid–solid mass transfer coefficients per phase, i.e., $(k_{ls}a_{ls})^g$ and $(k_{ls}a_{ls})^l$. One of the terms will decrease with increasing gas velocity whereas the other will increase with increasing gasvelocity, resulting in the minimum which is observed for $k_{ls}a_{ls}$.

Jadhav and Pangarkar,[22] and Goto et al.[23] measured k_{ls} for Raschig and Pall rings and spherical particles, respectively. They observed that k_{ls} increases with increasing gas velocity and increasing liquid velocity. Typical values for k_{ls} for cocurrent gas–liquid flow through packed beds are in the order of magnitude of 10^{-5} to 10^{-4} m_l^3 m_i^{-2} s^{-1}.[22,24,25] For structured packings consisting of corrugated sheets, k_{ls} has been found to be in the order of magnitude of 5×10^{-7} to 5×10^{-5} m_l^3 m_i^{-2} s^{-1}.[3,13,14] The values of k_{ls} in this work range from 5.5×10^{-6} to 8.2×10^{-4} m_l^3 m_r^{-2} s^{-1}. These values of k_{ls} for 10 PPI and 20 PPI solid foam are in the same range as found for random packings for both liquid velocities. The values of k_{ls} for 40 PPI solid foam and a liquid velocity of 0.04 m_l^3 m_r^{-2} s^{-1} are also in the range of the random packings. The values of k_{ls} for 40 PPI solid with $u_l = 0.02$ m_l^3 m_r^{-2} s^{-1} and $u_g \geq 0.4$ m_g^3 m_r^{-2} s^{-1}, are slightly below the values found in literature for random packings, but in the same range as found for corrugated sheet packings.

The initial decrease of k_{ls} with increasing gas velocity is in contrast with the data found in literature for k_{ls} in packed beds. Jadhav and Pangarkar,[22] Trivizadakis and Karabelas,[24] Nikov and Delmas,[25] and Hassan et al.[26] observed an increase of k_{ls} with increasing gas velocity. Jadhav and Pangarkar[22] observed a constant k_{ls} for Raschig rings and gas velocities exceeding 0.25 m_g^3 m_r^{-2} s^{-1}. They attributed this to the presence of large gas slugs, which do not contribute significantly to the liquid phase turbulence. Stemmet et al.[10] observed a flow transition from bubbly flow to pulse flow at a gas velocity of 0.3 m_g^3 m_r^{-2} s^{-1}. In this work, the pulse flow was observed for $u_g \geq 0.4$ m_g^3 m_r^{-2} s^{-1}. The local minimum of k_{ls} is located at $u_g = 0.6$ m_g^3 m_r^{-2} s^{-1} for all cases.

In the pulse flow regime, the liquid–solid mass transfer in the gas phase will take place through the stagnant liquid film on the solid foam, resulting in relatively low liquid–solid mass transfer rates. In the liquid pulse, the liquid flow

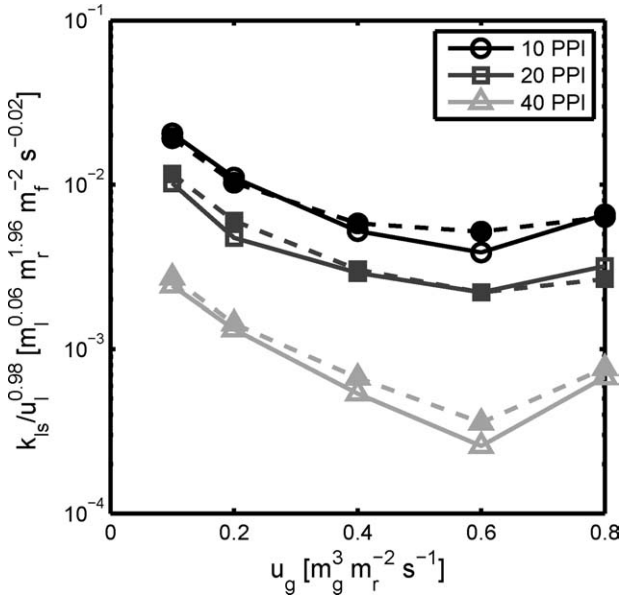

Figure 8. Ratio of k_{ls} and $u_l^{0.98}$ as a function of gas velocity.

The open symbols with the solid lines correspond to u_l = 0.02 m_l^3 m_r^{-2} s^{-1} and the closed symbols with the dashed lines correspond to u_l = 0.04 m_l^3 m_r^{-2} s^{-1}. For both liquid, velocities, the data points coincide for the individual PPI numbers, thus eliminating the effect of liquid velocity.

around the struts generates turbulence, enhancing the liquid–solid mass transfer rate. The gas holdup varies only marginally with increasing gas velocity (Figure 6b) for the pulse flow regime. This implies that the velocity of the liquid pulses increase with increasing gas velocity. The increase of liquid-pulse velocity results in an increase of k_{ls}. In the gas phase, the film layer thickness remains approximately constant, resulting an approximately constant liquid–solid mass transfer coefficient in the gas-phase. The liquid–solid mass transfer coefficient decreases for increasing gas holdup (or decreasing liquid holdup), i.e., increasing gas velocity. The decrease of k_{ls} with decreasing liquid holdup indicates that the liquid–solid mass transfer mainly takes place in the bulk liquid. In the pulse flow regime, the higher interstitial liquid velocity increases with increasing gas velocity. Resulting in an increase of k_{ls} with increasing gas velocity, and thus resulting in a minimum value for k_{ls}.

Figure 7b shows that k_{ls} increases with increasing liquid velocity. The effect of liquid velocity on k_{ls} is approximately the same for all gas velocities. Literature shows that k_{ls} is proportional to u_l^n, where various values for n have been found, typically ranging from 0.34 to 0.8.[22–24,26–28] Rode et al.[28] recalculated the correlation of Specchia et al.[29] to include the interstitial Reynolds number into the correlation, and found a value of 1.244 for n. The value of n for the data shown in Figure 7b was determined by fitting the data to the following relation:

$$k_{ls,0.02} = k_{ls,0.04}\left(\frac{0.02}{0.04}\right)^n \tag{16}$$

where $k_{ls,0.02}$ and $k_{ls,0.04}$ are the intrinsic liquid–solid mass transfer coefficient at u_l = 0.02 and 0.04 m_l^3 m_r^{-2} s^{-1}, respectively. A value of 0.98 ± 0.09 was obtained for n. Figure 8 shows the ratio $k_{ls}/u_l^{0.98}$ as a function of gas velocity. The graph shows that for both liquid velocities, $k_{ls}/u_l^{0.98}$ coincides for the individual PPI numbers. The effect of liquid velocity on k_{ls} is thus the same for all the gas velocities studied. The value of 0.98 for n is relatively high compared to the values found in literature for packings. Values up to 0.936 have been found for n in case of turbulent single phase flow through pipes.[30] Possibly, the size of struts limits the length of the mass transfer and hydrodynamic boundary layer. Also, the passage of gas bubbles can disrupt the formation of a boundary layer. The dependency of this reduced boundary layer thickness on the liquid velocity could be close to the dependency found for turbulent flow in pipes which is close to the exponent 0.98 found in this work.

The sensitivity of $k_{ls}a_{ls}$ to the used values of $(k_{gl}a_{gl})_{foam}$ and $(k_{gl}a_{gl})_{L_1}$ has been assessed by calculating $k_{ls}a_{ls}$ for different values of $(k_{gl}a_{gl})_{foam}$ and $(k_{gl}a_{gl})_{L_1}$. The sensitivity of $k_{ls}a_{ls}$ to $(k_{gl}a_{gl})_{foam}$ and $(k_{gl}a_{gl})_{L_1}$ is shown in Figure 9 for 10 PPI foam with a liquid velocity of 0.02 m_l^3 m_r^{-2} s^{-1}. The open symbols connected by the solid line correspond to the original data, the dashed line correspond to changes in $(k_{gl}a_{gl})_{foam}$ by ±50%, and the dash–dot line corresponds to a reduction of $(k_{gl}a_{gl})_{L_1}$ by 50%. The gas–liquid mass transfer coefficient of the catalytic foam piece, $(k_{gl}a_{gl})_{foam}$, has a significant influence on $k_{ls}a_{ls}$. For the catalytic foam piece, gas–liquid and liquid solid mass transfer take place in series. Therefore, if $(k_{gl}a_{gl})_{foam}$ increases, also $k_{ls}a_{ls}$ increases to match the dissolved oxygen concentration at the exit of the

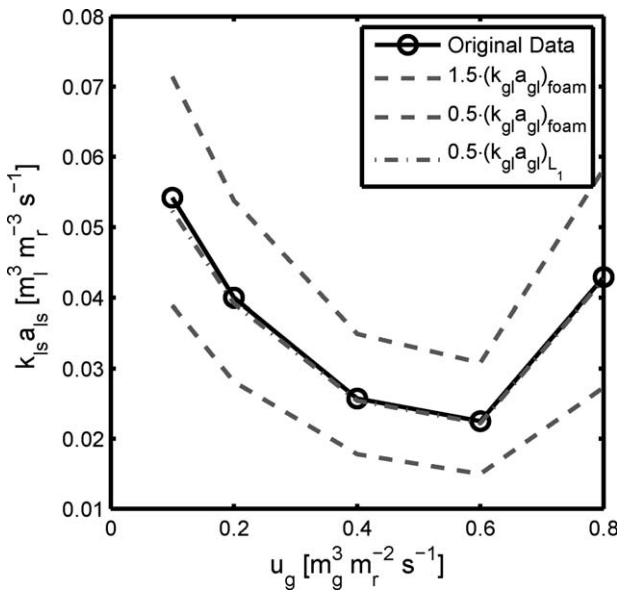

Figure 9. Sensitivity plot for the liquid–solid mass transfer coefficient as a function of gas velocity for 10 PPI solid foam with u_l = 0.02 m_l^3 m_r^{-2} s^{-1}.

The solid line corresponds to the original data, the gray dashed lines correspond to 1.5 and 0.5 times $(k_{gl}a_{gl})_{foam}$, and the gray dash–dot line corresponds to 0.5 times $(k_{gl}a_{gl})_{L_1}$. The value of $(k_{gl}a_{gl})_{L_1}$ has a minor effect on the determination of $k_{ls}a_{ls}$. The value of $(k_{gl}a_{gl})_{foam}$ shows a significant influence on the value of $k_{ls}a_{ls}$. Changing $(k_{gl}a_{gl})_{foam}$ by 50% results in a change of maximum 37% in $k_{ls}a_{ls}$.

reactor. For the data shown in Figure 9, changing $(k_{gl}a_{gl})_{foam}$ by 50% results in a maximum change of 37% in $k_{ls}a_{ls}$. Figure 9 shows that $k_{ls}a_{ls}$ is not sensitive to $(k_{gl}a_{gl})_{L_1}$. The value of $(k_{gl}a_{gl})_{L_1}$, determines the dissolved oxygen concentration at the entrance of the catalytic foam piece, C_l^m. The low sensitivity towards $(k_{gl}a_{gl})_{L_1}$ shows that C_l^m does not vary significantly with varying $(k_{gl}a_{gl})_{L_1}$. For all cases reducing the $(k_{gl}a_{gl})_{L_1}$ by 50% resulted in values of C_l^m, which were at least 92% of the saturation concentration.

Conclusions

In this article we studied the liquid–solid mass transfer for cocurrent gas–liquid upflow through solid foam catalyst supports. The effects of gas velocity, liquid velocity, and PPI number have been studied. The following conclusions can be drawn:

1. The liquid–solid mass transfer coefficient, k_{ls}, increases with increasing liquid velocity. k_{ls} was found to be proportional to $u_l^{0.98}$.

2. The liquid–solid mass transfer coefficient, k_{ls}, initially decreases with increasing gas velocity and after reaching a minimum value increases with increasing gas velocity. k_{ls} ranges from 5.5×10^{-6} to 8×10^{-4} m_l^3 m_r^{-2} s^{-1}.

3. The volumetric liquid–solid mass transfer coefficient, $k_{ls}a_{ls}$, is approximately the same for 10 PPI and 20 PPI foam, ranging from 2×10^{-2} to 9×10^{-2} m_l^3 m_r^{-3} s^{-1}. For 40 PPI foam lower values of $k_{ls}a_{ls}$ were found, ranging from 6×10^{-3} to 4×10^{-2} m_l^3 m_r^{-3} s^{-1}.

4. The calculation of $k_{ls}a_{ls}$ from experimental data is very robust towards the value of the gas–liquid mass transfer coefficient of the foam piece without catalyst preceding the foam piece with catalyst. However, $k_{ls}a_{ls}$ is sensitive to errors in the value of the gas–liquid mass transfer coefficient of the solid foam with catalyst, $(k_{gl}a_{gl})_{foam}$. An error of 50% in $(k_{gl}a_{gl})_{foam}$ results in a maximum error of 37% in $k_{ls}a_{ls}$.

5. The values found for k_{ls} are in the same range as found for random packing and structured packings.

Acknowledgments

The authors are grateful to Prof. Hugh Stitt and Dr. Alison Wagland from Johnson Matthey for providing the Pd/γ-alumina washcoated solid foam samples. The authors gratefully acknowledge the financial support from the Dutch Technology Foundation STW (Project EPC.6601), Stork-Veco, Recemat, Shell Global Solutions International B.V., DSM Research B.V, BASF Nederland B.V., and Schering-Plough.

Notation

a_f = specific surface area of the solid foam m_f^2 m_r^{-3}
a_{ls} = liquid–solid interfacial area per unit reactor volume m_i^2 m_r^{-3}
a_{ls}^g = liquid–solid interfacial area per unit gas volume m_i^2 m_g^{-3}
a_{ls}^l = liquid–solid interfacial area per unit liquid volume $m_i^2 m_l^{-3}$
C_g = gas phase concentration mol m_g^{-3}
C_g^i = gas phase concentration at the inlet of the column mol m_g^{-3}
C_g^m = gas phase concentration at the inlet of the catalytic solid foam mol m_g^{-3}
C_l = liquid phase concentration mol m_l^{-3}
C_l^i = liquid phase concentration at the inlet of the column mol m_l^{-3}
C_l^m = liquid phase concentration of the catalytic solid foam mol m_l^{-3}
D_p = pore diameter m_f
H = henry coefficient m_l^3 m_g^{-3}
$(k_{ls}a_{ls})^g$ = volumetric liquid–solid mass transfer coefficient on gas volume basis m_l^3 m_g^{-3} s^{-1}
$(k_{ls}a_{ls})^l$ = volumetric liquid–solid mass transfer coefficient on liquid volume basis s^{-1}
k_r = intrinsic reaction rate coefficient m_l^3 mol_{cat}
$k_{gl}a_{gl}$ = volumetric gas–liquid mass transfer coefficient m_l^3 $m_r^{-3}{\cdot}s^{-1}$
$k_{ls}a_{ls}$ = volumetric liquid–solid mass transfer coefficient m_l^3 $m_r^{-3}{\cdot}s^{-1}$
L = solid foam packing height mol m_l^{-3}
L_t = weight specific amount of atoms of the catalyst mol_{cat} kg_{sup}
N_{PPI} = PPI number pores $inch^{-1}$
R_v = reaction rate per unit volume reactor mol m_r^{-3} s^{-1}
u_g = superficial gas velocity m_g^3 m_r^{-2} s^{-1}
u_l = superficial liquid velocity m_l^3 m_r^{-2} s^{-1}
z = spatial reactor coordinate m

Greek letters

α = parameter used in Eq. 9: $k_{gl}a_{gl}/u_gH$ m_r^{-1}
β = parameter used in Eq. 9: $(k_{gl}a_{gl}/u_l) + (k_{ls}a_{ls}/u_l) \times \left(1 - \frac{k_{ls}a_{ls}}{k_r L_t \rho_{sup} \varepsilon_{sup} + k_{ls}a_{ls}}\right)$ m_r^{-1}
ε_f = porosity of the solid foam m_{void}^3 m_r^{-3}
ε_g = gas holdup; $\varepsilon_g = \varepsilon_f - \varepsilon_l$ m_g^3 m_r^{-3}
ε_{sup} = holdup of the support m_{sup}^3 m_r^{-3}
γ = parameter used in Eq. 9: $k_{gl}a_{gl}/u_l$ m_r^{-1}
η = effectiveness factor
ρ_{sup} = density of the support kg_{sup} m_{sup}^{-2}

Literature Cited

1. Cybulski A, Albers RE, Moulijn JA. *Monolithic catalysts for three-phase processes*. In: Cybulski A, Moulijn JA, editors. *Structured Catalysts and Reactors*, 2nd ed. Volume 110 of *Chemical Industries*, chapter 10 Wassaw, Poland; CRC, CHEMIPAN, Institute of Physical Chemistry, Polish Academy of Sciences, 2006:355–391.
2. Bailer O, Spiegel L, van Scala C. *Structured packings for reactive distillation*. In: Cybulski A, Moulijn JA, editors. *Structured Catalysts and Reactors*, 2nd ed. Volume 110 of *Chemical Industries*. chapter 15. Winterthur, Switzerland: CRC, Sulzer Chemtech Ltd, 2006: 539–550.
3. Higler AP, Krishna R, Ellenberger J, Taylor R. Counter-current operation of a structured catalytically packed-bed reactor: liquid phase mixing and mass transfer. *Chem Eng Sci*. 1999;54:5145–5152.
4. Matatov-Meytal Y, Sheintuch M. Catalytic fibers and cloths. *Appl Catal A*. 2002;231:1–16.
5. Trubac RE, Dautzenberg FM, Griffin TA, Paikert B, Schmidt VR, Overbeek RA. Micro-engineered catalyst systems: Abb's advancement in structured catalytic packings. *Catal Today*. 2001;69:17–24.
6. Pangarkar K, Schildhauer TJ, van Ommen JR, Nijenhuis J, Kapteijn F, Moulijn JA. Structured Packings for Multiphase Catalytic reactors. *Ind Eng Chem Res*. 2008;47:3720–3751.
7. Wenmakers PWAM, van der Schaaf J, Kuster BFM, Schouten JC. "Hairy foam": carbon nanofibers grown on solid carbon foam. A fully accessible, high surface area, graphitic catalyst support. *J Mater Chem*. 2008;18:2426–2436.
8. Stemmet CP, Jongmans JN, van der Schaaf J, Kuster BFM, Schouten JC. Hydrodynamics of gas–liquid counter-current flow in solid foam packings. *Chem Eng Sci*. 2005;60:6422–6429.
9. Stemmet CP, van der Schaaf J, Kuster BFM, Schouten JC. Solid foam packings for multiphase reactors: modeling of liquid holdup and mass transfer. *Chem Eng Res Des*. 2006;84:1134–1141.
10. Stemmet CP, Meeuwse M, van der Schaaf J, Kuster BFM, Schouten JC. Gas–liquid mass transfer and axial dispersion in solid foam packings. *Chem Eng Sci*. 2007;62:5444–5450.
11. Twigg MV, Richardson JT. Fundamentals and applications of structured ceramic foam catalysts. *Ind Eng Chem Res*. 2007;46:4166–4177.
12. Incera Garrido G, Patcas FC, Lang S, Kraushaar-Czarnetzki B. Mass transfer and pressure drop in ceramic foams: a description for different pore sizes and porosities. *Chem Eng Sci*. 2008;63:5202–5217.
13. Baten JM, Krishna R. Liquid-phase mass transfer within katapak-s structures studied using computational fluid dynamics simulations. *Catal Today*. 2001;69:371–377.
14. Battista J, Boehm U. Mass transfer in trickle-bed reactors with structured packing. *Chem Eng Technol*. 2003;26:1061–1067.
15. Langlois S, Coeuret F. Flow-through and flow-by porous electrodes of nickel foam. II. Diffusion-convective mass transfer between the electrolyte and the foam. *J Appl Electrochem*. 1989;19:51–60.

16. Luo D, Ghiaasiaan SM. Interphase mass transfer in cocurrent vertical two-phase channel flows with non-newtonian liquids. *Int Comm Heat Mass Transfer*. 1997;24:1–10.
17. Kluytmans JHJ, Markusse AP, Kuster BFM, Marin GB, Schouten JC. Engineering aspects of the aqueous noble metal catalysed alcohol oxidation. *Catal Today*. 2000;57:143–155.
18. Ruthiya KC, van der Schaaf J, Kuster BFM, Schouten JC. Modeling the effect of particle-to-bubble adhesion on mass transport and reaction rate in a stirred slurry reactor: influence of catalyst support. *Chem Eng Sci*. 2004;59:5551–5558.
19. Ruthiya KC. Mass Transfer and Hydrodynamics in Catalytic Slurry Reactors. Thesis/dissertation, Eindhoven University of Technology, 2005.
20. Ramachandran PA, Chaudhari RV. *Fixed-bed reactor with cocurrent upflow*. In: Hughes R, editor. *Three Phase Catalytic Reactors*, 1st ed. Volume 2 of Topics in Chemical Engineering, book chapter 8. New York: Gordon & Breach, Science Publishers, Inc., 1983.
21. Wenmakers PWAM, van der Schaaf J, Kuster BFM, Schouten JC. Enhanced liquid–solid mass transfer by carbon nanofibers on solid foam as catalyst support. *Chem Eng Sci*. 2010;65:247–254.
22. Jadhav SV, Pangarkar VG. Solid–liquid mass trasnfer in packed bubble columns. *Chem Eng Sci*. 1990;45:1139–1143.
23. Goto S, Levec J, Smith JM. Mass transfer in packed beds with two-phase flow. *Ind Eng Chem Process Des Dev*. 1975;14:473–478.
24. Trivizadakis ME, Karabelas AJ. A study of local liquid/solid mass transfer in packed beds under trickling and induced pulsing flow. *Chem Eng Sci*. 2006;61:7684–7696.
25. Nikov I, Delmas H. Solid–liquid mass transfer in three-phase fixed and fluidized beds. *Chem Eng Sci*. 1987;42:1089–1093.
26. Hassan I, Zahran RR, Mansour IS, Sedahmed GH. Liquid–solid mass transfer at a fixed bed of lessing rings, in relation to electrochemical reactor design. *Ind Eng Chem Res*. 2005;44:5761–5767.
27. Noseir SA, El-Kayar A, Farag HA, Sedahmed GH. Solid–liquid mass transfer at gas sparged fixed bed of rasching rings. *Int Comm Heat Mass Transfer*. 1997;24:733–740.
28. Rode S, Midoux N, Latifi MA, Storck A. Hydrodynamics and liquid–solid mass transfer mechanisms in packed beds operating in cocurrent gas–liquid downflow: an experimental study using electrochemical shear rate sensors. *Chem Eng Sci*. 1994;49:1383–1401.
29. Specchia V, Baldi G, Gianetto A. Solid–liquid mass transfer in concurrent two-phase flow through packed beds. *Ind Eng Chem Proc Des Dev*. 1978;17:362–367.
30. Harriott P, Hamilton RM. Solid–liquid mass transfer in turbulent pipe flow. *Chem Eng Sci*. 1965;20:1073–1078.

Appendix: Derivation

In this Appendix, the derivation for the dissolved oxygen concentration profile through the catalytic foam piece is presented (Figure 2). Assuming plug flow for both the gas and liquid phases, the mole balances of both phases are:

$$-u_l\frac{dC_l}{dz}+(k_{gl}a_{gl})_{foam}\left(\frac{C_g}{H}-C_l\right)-k_{ls}a_{ls}(C_l-C_s)=0 \quad \text{Liquid phase} \quad (A1)$$

$$-u_g\frac{dC_g}{dz}-(k_{gl}a_{gl})_{foam}\left(\frac{C_g}{H}-C_l\right)=0 \quad \text{Gas phase} \quad (A2)$$

with the following initial conditions:

$$z=0 \quad C_l=C_l^m \quad (A3)$$

$$z=0 \quad C_g=C_g^m \quad (A4)$$

For steady state conditions, the liquid–solid mass transfer rate is equal to the chemical reaction rate (Eq. 7) and the liquid–solid interfacial concentration, C_s, can then be determined as follows:

$$C_s=\frac{k_{ls}a_{ls}}{k_{ls}a_{ls}+\eta k_r L_t\rho_{sup}\varepsilon_{sup}}C_l \quad (A5)$$

Taking the Laplace transform of Eq. A2 and rearranging yields:

$$s\frac{\widehat{C}_g}{H}-\frac{C_g^m}{H}+\frac{k_{gl}a_{gl}}{u_gH}\left(\frac{\widehat{C}_g}{H}-\widehat{C}_l\right)=0 \quad (A6)$$

Using $\alpha=(k_{gl}a_{gl})_{foam}/u_gH$ and isolating $\widehat{C}_g/H$ results in:

$$\frac{\widehat{C}_g}{H}=\frac{C_g^m}{H}\frac{1}{s+\alpha}+\widehat{C}_l\frac{\alpha}{s+\alpha} \quad (A7)$$

Substitution of Eq. A5 into Eq. A1, rearranging, and taking the Laplace transform yields:

$$s\widehat{C}_l-C_l^m-\frac{(k_{gl}a_{gl})_{foam}}{u_l}\left(\frac{\widehat{C}_g}{H}-\widehat{C}_l\right)+\frac{k_{ls}a_{ls}}{u_l}\widehat{C}_l\left(1-\frac{k_{ls}a_{ls}}{k_rL_t\rho_{sup}\varepsilon_{sup}+k_{ls}a_{ls}}\right)=0 \quad (A8)$$

Combining Eqs. A7 and A8 results in:

$$s\widehat{C}_l-C_l^m-\frac{(k_{gl}a_{gl})_{foam}}{u_l}\left(\frac{C_g^m}{H}\frac{1}{s+\alpha}+\widehat{C}_l\frac{\alpha}{s+\alpha}-\widehat{C}_l\right)+\frac{k_{ls}a_{ls}}{u_l}\widehat{C}_l\left(1-\frac{k_{ls}a_{ls}}{k_rL_t\rho_{sup}\varepsilon_{sup}+k_{ls}a_{ls}}\right)=0 \quad (A9)$$

Isolating $\widehat{C}_l$ gives:

$$\widehat{C}_l=\left(C_l^m+\frac{(k_{gl}a_{gl})_{foam}}{u_l}\frac{C_g^m}{H}\frac{1}{s+\alpha}\right)\times\left[s-\frac{(k_{gl}a_{gl})_{foam}}{u_l}\frac{\alpha}{s+\alpha}+\frac{(k_{gl}a_{gl})_{foam}}{u_l}+\frac{k_{ls}a_{ls}}{u_l}\left(1-\frac{k_{ls}a_{ls}}{k_rL_t\rho_{sup}\varepsilon_{sup}+k_{ls}a_{ls}}\right)\right]^{-1} \quad (A10)$$

The term in the square brackets of Eq. A10 can be rewritten as:

$$\left[s-\frac{\alpha\gamma}{s+\alpha}+\beta\right]=\frac{1}{s+\alpha}\left[\left(s+\frac{1}{2}(\alpha+\beta)\right)^2-\frac{1}{4}(\alpha+\beta)^2-\alpha(\gamma-\beta)\right]= \quad (A11)$$

$$\frac{1}{s+\frac{1}{2}(\alpha+\beta)+\frac{1}{2}(\alpha-\beta)}\times\left[\left(s+\frac{1}{2}(\alpha+\beta)\right)^2-\frac{1}{4}(\alpha+\beta)^2-\alpha(\gamma-\beta)\right] \quad (A12)$$

with:

$$\beta = \frac{(k_{gl}a_{gl})_{foam}}{u_l} + \frac{k_{ls}a_{ls}}{u_l}\left(1 - \frac{k_{ls}a_{ls}}{k_r L_t \rho_{sup}\varepsilon_{sup} + k_{ls}a_{ls}}\right)$$

$$\gamma = \frac{(k_{gl}a_{gl})_{foam}}{u_l}$$

Combing Eq. A12 with the first term in the round brackets of Eq. A10 yields:

$$C_l^m\left(\frac{s + \frac{1}{2}(\alpha+\beta)}{\left(s + \frac{1}{2}(\alpha+\beta)\right)^2 - \frac{1}{4}(\alpha+\beta)^2 - \alpha(\gamma-\beta)} + \frac{\frac{1}{2}(\alpha-\beta)}{\left(s + \frac{1}{2}(\alpha+\beta)\right)^2 - \frac{1}{4}(\alpha+\beta)^2 - \alpha(\gamma-\beta)}\right) \quad \text{(A13)}$$

Taking the inverse Laplace transform results in:

$$C_l^m e^{-\frac{1}{2}(\alpha+\beta)z}\left(\cos h\left(z\sqrt{\frac{1}{4}(\alpha+\beta)^2 + \alpha(\gamma-\beta)}\right) + \ldots\frac{1}{2}(\alpha-\beta)\frac{\sin h\left(z\sqrt{\frac{1}{4}(\alpha+\beta)^2 + \alpha(\gamma-\beta)}\right)}{\sqrt{\frac{1}{4}(\alpha+\beta)^2 + \alpha(\gamma-\beta)}}\right) \quad \text{(A14)}$$

Combining term A11 with the second term in the round brackets of Eq. A10 yields:

$$\frac{\gamma\frac{C_g^m}{H}}{\left(s + \frac{1}{2}(\alpha+\beta)\right)^2 - \frac{1}{4}(\alpha+\beta)^2 - \alpha(\gamma-\beta)} \quad \text{(A15)}$$

Taking the inverse Laplace transform yields:

$$\gamma\frac{C_g^m}{H}e^{-\frac{1}{2}(\alpha+\beta)z}\frac{\sin h\left(z\sqrt{\frac{1}{4}(\alpha+\beta)^2 + \alpha(\gamma-\beta)}\right)}{\sqrt{\frac{1}{4}(\alpha+\beta)^2 + \alpha(\gamma-\beta)}} \quad \text{(A16)}$$

Combining terms A14 and A16 gives:

$$C_l = e^{-\frac{1}{2}(\alpha+\beta)z}\left[C_l^m \cos h\left(z\sqrt{\frac{1}{4}(\alpha+\beta)^2 + \alpha(\gamma-\beta)}\right) + \quad \text{(A17)}$$

$$\left(\frac{1}{2}C_l^m(\alpha-\beta) + \frac{C_g^m}{H}\gamma\right)\frac{\sin h\left(z\sqrt{\frac{1}{4}(\alpha+\beta)^2 + \alpha(\gamma-\beta)}\right)}{\sqrt{\frac{1}{4}(\alpha+\beta)^2 + \alpha(\gamma-\beta)}}\Bigg] \quad \text{(A18)}$$

This relation describes the dissolved gas concentration profile in the catalytic foam piece as a function of gas and liquid velocity, gas–liquid mass transfer, liquid–solid mass transfer, and kinetics. Using experimentally determined dissolved gas concentrations and knowing the gas–liquid mass transfer coefficient, this relation can be used to determine the liquid–solid mass transfer coefficient for mass transfer limited reactions.

Manuscript received Aug. 31, 2009, and final revision received Feb. 4, 2010.